6310 *Chem. Mater.* **2010,** *22,* 6310–6318
DOI:10.1021/cm102074w

CHEMISTRY OF MATERIALS
Article

Synthesis of Bimetallic Au@Pt Nanoparticles with Au Core and Nanostructured Pt Shell toward Highly Active Electrocatalysts

Hamed Ataee-Esfahani,[†,‡] Liang Wang,*[,†] Yoshihiro Nemoto,[†] and Yusuke Yamauchi*[,†,‡,§]

[†]*World Premier International (WPI) Research Center for Materials Nanoarchitectonics, National Institute for Materials Science, 1-1 Namiki, Tsukuba 305-0044, Japan,* [‡]*Faculty of Science and Engineering, Waseda University, 3-4-1 Ohkubo, Shinjuku 169-8555, Japan, and* [§]*Precursory Research for Embryonic Science and Technology (PRESTO), Japan Science and Technology Agency (JST), 4-1-8 Honcho, Kawaguchi, Saitama 332-0012, Japan*

Received July 26, 2010. Revised Manuscript Received October 11, 2010

Au@Pt nanocolloids with nanostructured dendritic Pt shells are successfully synthesized by chemically reducing both H_2PtCl_6 and $HAuCl_4$ species in the presence of a low-concentration surfactant solution. By applying an ultrasonic treatment, the particle size of the Au@Pt nanocolloids is dramatically decreased and their size distribution becomes very narrow. The difference in reduction potentials of the two soluble metal salts (Au(III) and Pt(IV) species) plays a key role in the one-step synthesis of the core−shell structure. Because of the different reduction potentials, the reduction of Au ions preferentially occurs over a short time to form the Au seeds. It is followed by overgrowth of Pt nanodendritic nanowires on the Au seeds, which is confirmed by ultraviolet−visible light absorption spectroscopy and transmission electron microscopy. Interestingly, the Pt shell thicknesses on Au cores can be easily tuned by controlling the Pt/Au molar ratios in the starting precursor solutions. Through the optimization of the Pt shell thicknesses, the Au@Pt nanocolloids can exhibit enhanced activity as an electrocatalyst for a methanol oxidation reaction, which will be important to improve the utilization efficiency of Pt catalysts in the future.

1. Introduction

Currently, nanoporous/mesoporous inorganic materials with high surface area have been prepared through a self-assembly process of surfactants,[1−4] and they are expected to be utilized for many applications such as adsorbent materials and catalytic supports. Nanoporous materials with controlled compositions, different types of nanostructures, different pore sizes, and various morphologies have been extensively investigated during recent decades. Especially, the compositions strongly govern the materials' properties. Recently, the possible compositions have been drastically extended to not only silica but also carbon, inorganic−organic hybrids, polymers, and even metals.[5−10] Nanoporous metals are considerably interesting, because we can expect huge electrochemical applications, such as methanol oxidation reaction and oxygen reduction reaction, which are not attainable by other compositions.[10] Among all of the metal compositions, especially Pt and Pt-based nanostructures with high surface area and desired utilization efficiency have attracted a great deal of attention, because of their unique catalytic activities.[11−16] Because of the high cost of Pt, optimizing both the size and shape of Pt nanostructures is necessary to reduce Pt loading.[17,18] To date, various Pt nanostructures, such as nanospheres,[19]

*Authors to whom correspondence should be addressed. E-mails: Wang.Liang@nims.go.jp (L.W.) and Yamauchi.Yusuke@nims.go.jp (Y.Y.).

(1) Yanagisawa, T.; Shimizu, T.; Kuroda, K.; Kato, C. *Bull. Chem. Soc. Jpn.* **1990**, *63*, 988.
(2) Kresge, C. T.; Leonowicz, M. E.; Roth, W. J.; Vartuli, J. C.; Beck, J. S. *Nature* **1992**, *359*, 710.
(3) Inagaki, S.; Fukushima, Y.; Kuroda, K. J. *Chem. Soc. Chem. Commun.* **1993**, 680.
(4) Zhao, D. Y.; Feng, J. L.; Huo, Q. S.; Melosh, N.; Fredrickson, G. H.; Chmelka, B. F.; Stucky, G. D. *Science* **1998**, *279*, 548.
(5) Guo, L. M.; Cui, X. Z.; Li, Y. S.; He, Q. J.; Zhang, L. X.; Bu, W. B.; Shi, J. L. *Chem. Asian J.* **2009**, *4*, 1480.
(6) Gao, L.; Wei, F.; Zhou, Y.; Fan, X. X.; Wang, Y.; Zhu, J. H. *Chem. Asian J.* **2009**, *4*, 587.
(7) Huang, Y.; Cai, H. Q.; Yu, T.; Sun, X. L.; Tu, B.; Zhao, D. Y. *Chem. Asian J.* **2007**, *2*, 1282.
(8) Wan, Y.; Zhang, D. Q.; Zhai, Y. P.; Feng, C. M.; Chen, J.; Li, H. X. *Chem. Asian J.* **2007**, *2*, 875.
(9) Lu, A.-H.; Schüth, F. *Adv. Mater.* **2006**, *18*, 1793.
(10) Yamauchi, Y.; Kuroda, K. *Chem. Asian J.* **2008**, *3*, 664.
(11) Chen, J. Y.; Lim, B.; Lee, E. P.; Xia, Y. N. *Nano Today* **2009**, *4*, 81.
(12) Peng, Z. M.; Yang, H. *Nano Today* **2009**, *4*, 143.
(13) Tian, N.; Zhou, Z. Y.; Sun, S. G.; Ding, Y.; Wang, Z. L. *Science* **2007**, *316*, 732.
(14) Chen, J. Y.; Herricks, T.; Xia, Y. N. *Angew. Chem., Int. Ed.* **2005**, *44*, 2589.
(15) Sun, S. H.; Yang, D. Q.; Villers, D.; Zhang, G. X.; Sacher, E.; Dodelet, J. P. *Adv. Mater.* **2008**, *20*, 571.
(16) Wang, C.; Daimon, H.; Onodera, T.; Koda, T.; Sun, S. H. *Angew. Chem., Int. Ed.* **2008**, *47*, 3588.
(17) Song, Y.; Garcia, R. M.; Dorin, R. M.; Wang, H. R.; Qiu, Y.; Coker, E. N.; Steen, W. A.; Miller, J. E.; Shelnutt, J. A. *Nano Lett.* **2007**, *7*, 3650.
(18) Sun, Y.; Zhuang, L.; Lu, J.; Hong, X.; Liu, P. *J. Am. Chem. Soc.* **2007**, *129*, 15465.
(19) Bigall, N. C.; Hartling, T.; Klose, M.; Simon, P.; Eng, L. M.; Eychmuller, A. *Nano Lett.* **2008**, *8*, 4588.
(20) Song, Y. J.; Yang, Y.; Medforth, C. J.; Pereira, E.; Singh, A. K.; Xu, H. F.; Jiang, Y. B.; Brinker, C. J.; van Swol, F.; Shelnutt, J. A. *J. Am. Chem. Soc.* **2004**, *126*, 635.
(21) Wang, L.; Yamauchi, Y. *J. Am. Chem. Soc.* **2009**, *131*, 9152.

 Published on Web 11/04/2010

nanodendrites,[20−23] nanofibers/nanowires,[24,25] nanocages,[26] nanotubes,[27] and nanosheets,[28] have been successfully synthesized.

Currently, bimetallic core−shell nanospheres with a Pt shell have been widely studied. In comparison to Pt alone, such core−shell nanostructures not only improve the utilization efficiency of catalysts, but also reduce Pt usage in catalysts.[29−38] However, in all of these cases, complex procedures including at least two steps for the preparation of core−shell nanostructures with a dendritic Pt shell are proposed. Also, high-temperature and high-pressure conditions sometimes are required. Hence, the development of a facile and economic method for the one-step synthesis of core−shell nanostructures with a high Pt surface area is a challenging issue to be solved urgently. Another problem with the previous studies is that the size of the core−shell nanoparticles is widely distributed,[39] becoming impossible to finely control the Pt shell thicknesses on the cores. For the realization of extremely high diffusion of guest species from the outside, the Pt shell thicknesses should be effectively decreased. There is a reciprocal relationship between the Pt shell thicknesses and catalytic activity. Therefore, in the structure-sensitive electrocatalytic reactions, tailored core−shell nanoparticles with an ideal Pt shell thickness and narrow particle size distribution are especially vital.[18,31]

To overcome the above serious problems at the same time, here, we report a new synthetic route for bimetallic Au@Pt nanocolloids with a Au core and a dendritic Pt shell, by utilizing a surfactant-assisted process with an ultrasonic irradiation treatment. This synthetic approach enables the production of monodispersed Au@Pt nanocolloids in a wide range of the Pt precursor concentrations. It becomes possible to precisely control the Pt shell thicknesses on the Au cores. Through optimization of the Pt shell thicknesses, we can realize the highest utilization efficiency of the Pt, which is a very important finding for future design of a new type of electrocatalyst. Also, the distribution of the particle sizes is very narrow, and the effect of the ultrasonic irradiation on the particle size distribution is carefully discussed. We believe that our method is suitable for large-scale production of nanocatalysts, because it is a one-step, inexpensive method for the synthesis of uniform nanoparticles with high Pt surface area.

2. Experimental Section

2.1. Materials. H_2PtCl_6 and $HAuCl_4$ as metal sources were purchased from Nacalai Tesque, Inc. (Kyoto, Japan). Ascorbic acid (AA), which was used as a reducing agent, was purchased from Nacalai Tesque, Inc. (Kyoto, Japan). Pluronic F127 (M_w = 12600) was obtained from Sigma.

2.2. Synthesis of Au@Pt Spheres. In a typical synthesis of Au@Pt nanocolloids (Pt/Au molar ratio = 1.0), 3.0 mL of H_2PtCl_6 solution (20 mM) and 3.0 mL of $HAuCl_4$ solution (20 mM) were mixed with Pluronic F127 (0.06 g) in a small beaker. After that, 6.0 mL of AA solution (0.1 M) was added, and the mixture was then sonicated for 15 min. For a better understanding of the ultrasonic irradiation effect, in another experiment, the precursor solution after adding AA was mixed, using a magnetic stirrer, without the use of the ultrasonic treatment. After the reaction for 24 h, all the dissolved metal sources were completely deposited. The product was collected by centrifugation at 10 000 rpm for 20 min and residual Pluronic F127 was removed by three consecutive washing/centrifugation cycles with acetone and water. The collected product was dried at 45 °C for several days. For further characterization, the dried product was redispersed in water to produce a stable colloidal suspension.

For the preparation of the Au@Pt nanocolloids with different Pt shell thicknesses, Pt/Au molar ratios in the starting solution were varied from 0.0 to 4.0. The added amount of $HAuCl_4$ (20 mM) was fixed to 3 mL, while the added amount of H_2PtCl_6 (20 mM) was changed from 0.0 mL to 12.0 mL. The molar ratios of the added AA and F127 to the dissolved metal species were fixed. The compositional ratios in the starting solution are listed in Table 1.

The dendritic Pt nanocolloids without Au cores were prepared as follows. Three milliliters (3.0 mL) of H_2PtCl_6 solution (20 mM), containing 0.03 g of F127, was mixed with 3.0 mL of AA solution (0.1 M) and the mixture was sonicated for 15 min. After the reaction for 24 h, all the dissolved metal sources were completely deposited. The product was collected by centrifugation at 10 000 rpm for 20 min and residual Pluronic F127 was removed by three consecutive washing/centrifugation cycles with acetone and water. The collected product was dried at 45 °C for several days.

2.3. Characterization. Transmission electron microscopy (TEM) observation was performed using a JEOL Model JEM-2100F TEM system that was operated at 200 kV and equipped for energy-dispersive spectrometer (EDS) analysis. The sample for TEM characterization was prepared by depositing a drop of dilute suspensions on a carbon-coated copper grid and the sample was dried at room temperature. Wide-angle powder X-ray diffraction (XRD) patterns were obtained with a Rigaku Model Rint 2500X diffractometer that was using monochromated Cu Kα radiation (40 kV, 100 mA) and was operated using a step scan program (step width = 0.05°). Nitrogen adsorption−desorption data was obtained using a Belsorp 28 apparatus (Bel Japan, Inc.) at 77 K. Ultraviolet−visible light

(22) Wang, L.; Yamauchi, Y. *Chem. Mater.* **2009**, *21*, 3562.
(23) Wang, L.; Wang, H. J.; Nemoto, Y.; Yamauchi, Y. *Chem. Mater.* **2010**, *22*, 2835.
(24) Yamauchi, Y.; Takai, A.; Nagaura, T.; Inoue, S.; Kuroda, K. *J. Am. Chem. Soc.* **2008**, *130*, 5426.
(25) Takai, A.; Yamauchi, Y.; Kuroda, K. *J. Mater. Chem.* **2009**, *19*, 4205.
(26) Song, Y. J.; Garcia, R. M.; Dorin, R. M.; Wang, H. R.; Qiu, Y.; Shelnutt, J. A. *Angew. Chem., Int. Ed.* **2006**, *45*, 8126.
(27) Takai, A.; Yamauchi, Y.; Kuroda, K. *Chem. Commun.* **2008**, 4171.
(28) Song, Y. J.; Steen, W. A.; Peña, D.; Jiang, Y. B.; Medforth, C. J.; Huo, Q. S.; Pincus, J. L.; Qiu, Y.; Sasaki, D. Y.; Miller, J. E.; Shelnutt, J. A. *Chem. Mater.* **2006**, *18*, 2335.
(29) Koh, S.; Strasser, P. *J. Am. Chem. Soc.* **2007**, *129*, 12624.
(30) Whittingham, M. S.; Savinell, R. F.; Zawodzinski, T. *Chem. Rev.* **2004**, *104*, 4243.
(31) Zhao, D.; Xu, B. Q. *Angew. Chem., Int. Ed.* **2006**, *45*, 4955.
(32) Min, M.; Kim, C.; Yang, Y. I.; Yi, J.; Lee, H. *Phys. Chem. Chem. Phys.* **2009**, *11*, 9759.
(33) Zhao, D.; Xu, B. Q. *Phys. Chem. Chem. Phys.* **2006**, *8*, 5106.
(34) Kristian, N.; Wang, X. *Electrochem. Commun.* **2008**, *10*, 12.
(35) Lim, B.; Jiang, M. J.; Camargo, P. H. C.; Cho, E. C.; Tao, J.; Lu, X. M.; Zhu, Y. M.; Xia, Y. A. *Science* **2009**, *324*, 1302.
(36) Peng, Z. M.; Yang, H. *J. Am. Chem. Soc.* **2009**, *131*, 7542.
(37) Zhou, S. G.; McIlwrath, K.; Jackson, G.; Eichhorn, B. *J. Am. Chem. Soc.* **2006**, *128*, 1780.
(38) Wang, S. Y.; Kristian, N.; Jiang, S. P.; Wang, X. *Nanotechnology* **2009**, *20*, 025605.
(39) Ataee-Esfahani, H.; Wang, L.; Yamauchi, Y. *Chem. Commun.* **2010**, *46*, 3684.

Table 1. Compositional Ratios in the Starting Solution

sample	volume of H_2PtCl_6 solution (20 mM)	volume of $HAuCl_4$ solution (20 mM)	amount of F127	volume of AA solution (0.1 M)	Pt/Au molar ratio
1	0.0 mL	3.0 mL	0.03 g	3.0 mL	0.00
2	1.0 mL	3.0 mL	0.04 g	4.0 mL	0.33
3	2.0 mL	3.0 mL	0.05 g	5.0 mL	0.67
4	3.0 mL	3.0 mL	0.06 g	6.0 mL	1.0
5	6.0 mL	3.0 mL	0.09 g	9.0 mL	2.0
6	9.0 mL	3.0 mL	0.12 g	12 mL	3.0
7	12 mL	3.0 mL	0.15 g	15 mL	4.0

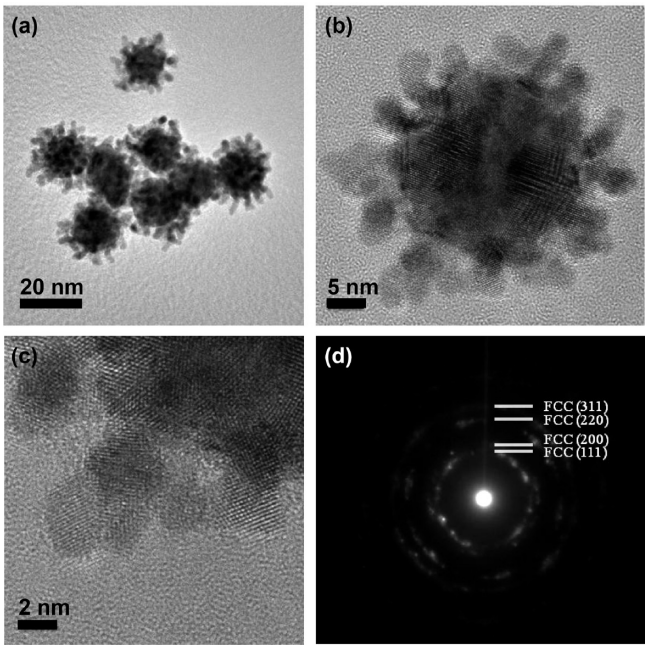

Figure 1. (a) Low-magnification and (b) high-magnification TEM images of Au@Pt nanocolloids prepared from a typical solution with a Pt/Au molar ratio of 1.0. (c) High-magnification TEM image of the Pt shell. (d) Selected-area electron diffraction (SAED) patterns taken from the Pt shell region.

(UV−vis) absorption spectra were recorded using a JASCO Model V-570 UV-vis-NIR spectrometer.

2.4. Electrochemical Measurements. Cyclic voltammogram (CV) experiments were performed using a CHI 842B electrochemical analyzer (CHI Instruments, USA). A conventional three-electrode cell was used, including an Ag/AgCl (saturated KCl) electrode as an reference electrode, a platinum wire as a counter electrode, and a modified glassy carbon electrode (GCE) (3 mm in diameter) as a working electrode. The modified GCE was coated with as-produced Au, Au@Pt, and Pt nanocolloids (4.0 μg) respectively. Then, they were dried at room temperature. Prior to electrochemical experiments, the electrodes with Au@Pt and Pt nanocolloids were cleaned electrochemically by cycling the electrode potential between −0.2 V and +1.6 V (vs Ag/AgCl) in 0.5 M H_2SO_4 until CVs that were characteristic for a clean Pt electrode were obtained. Methanol electro-oxidation measurements were performed in a solution of 0.5 M H_2SO_4 that contained 0.5 M methanol at a scan rate of 50 mV/s.

3. Results and Discussion

Figure 1 shows TEM images of the Au@Pt nanocolloids synthesized by ultrasonic-assisted method under the typical condition (the Pt/Au molar ratio used in the was is 1.0). The lower-magnification image (Figure 1a) indicates that the Au@Pt nanocolloids are strikingly uniform in morphology. The particle sizes were distributed in the range of 20−35 nm. No other isolated Pt or Au nanostructures were observed, demonstrating the high yield (~100%) synthesis of the Au@Pt nanocolloids. In all of the nanocolloids, a dark center was surrounded by a gray dendritic shell. This strong contrast revealed the formation of a core−shell structure (see Figures 1a and 1b). For further characterization of Au@Pt nanocolloids, high-resolution transmission electron microscopy (HRTEM) was applied to investigate the nanostructure and the lattice of an individual Pt shell (Figure 1c). The overgrowth of Pt dendritic nanowires on the Au core could be seen in the high-magnification TEM image. The Pt dendritic shells were composed of many interconnected nanowires 3 nm in diameter. The observed lattice fringes corresponded to the (111) planes of Pt face-centered cubic (fcc) crystals and they were randomly oriented over the entire area (Figure 1c). Selected-area electron diffraction (SAED) patterns of the Pt shells showed the ring patterns with intense spots assigned to (111), (200), (220), and (311) plane of Pt fcc crystals, showing the polycrystalline nature of Pt (Figure 1d). The elemental mapping as well as the line scanning also showed that the center of the particle is pure Au, whereas Pt is concentrated at the outer edge of the particle (see Figure 2). From the corresponding elemental mapping data, it was revealed that Pt and Au were distributed according to the morphology of the Au@Pt core−shell nanocolloids (see Figure 2c). This is direct evidence of the formation of an Au@Pt core−shell structure. The wide-angle XRD patterns of the Au@Pt core−shell nanocolloids showed both Au fcc and Pt fcc peaks, indicating the nonalloy structure (see Figure 3).

The essence of the synthesis of Au@Pt core−shell nanocolloids is to exploit the difference in standard reduction potentials of the two metal salts (H_2PtCl_6 and $HAuCl_4$). In the present system, $AuCl_4^-$ and $[PtCl_6]^{2-}$ could be reduced according to the following reactions:

$$AuCl_4^- + 3e^- \rightarrow Au + 4Cl^- \quad + 1.00 \text{ eV vs SHE} \tag{1}$$

$$[PtCl_6]^{2-} + 2e^- \rightarrow [PtCl_4]^{2-} + 2Cl^- \quad + 0.68 \text{ eV vs SHE} \tag{2}$$

$$[PtCl_4]^{2-} + 2e^- \rightarrow Pt + 4Cl^- \quad + 0.76 \text{ eV vs SHE} \tag{3}$$

The difference in the reduction potentials of the two soluble metal salts plays a key role in the one-step synthesis of a core−shell structure. Because of the large different

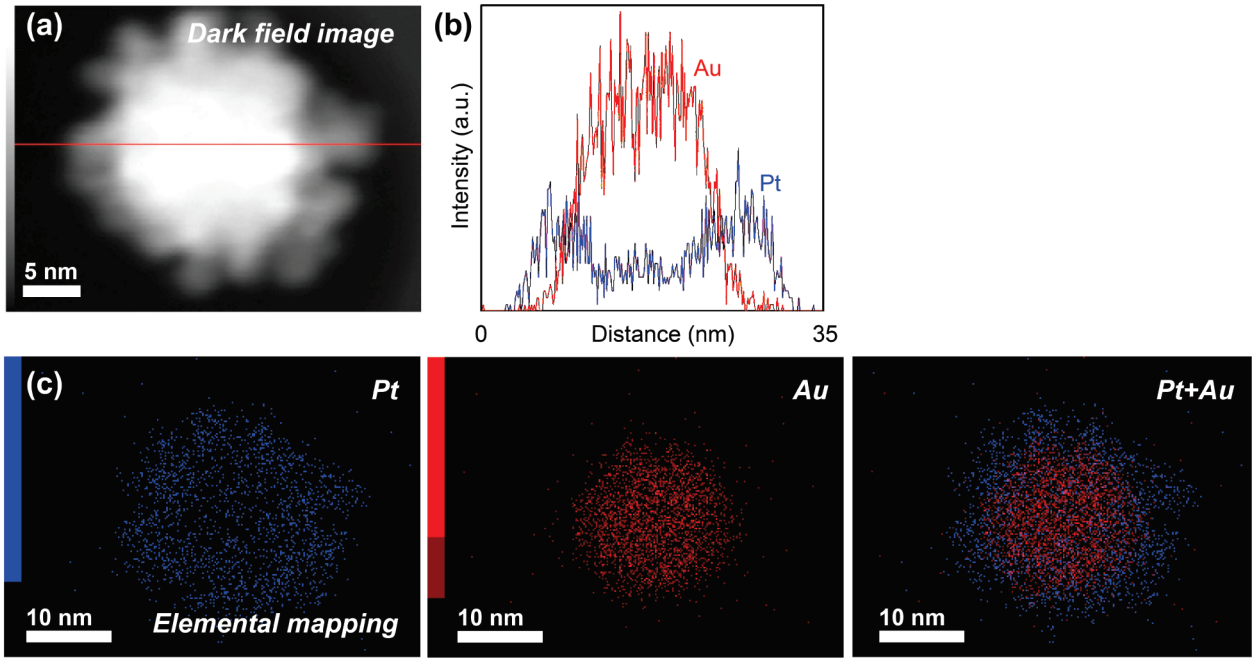

Figure 2. (a) High-angle annular dark-field scanning transmission electron microscopy (HAADF-STEM) image of Au@Pt nanocolloids prepared from a typical solution with a Pt/Au molar ratio of 1.0. (b) Elemental line scanning over the entire particle region indicated by the red line in panel (a). (c) Elemental mapping of the Au@Pt nanocolloids prepared from a typical solution with a Pt/Au molar ratio of 1.0. In panels (b) and (c), the red color indicates Au, whereas the blue color indicates Pt.

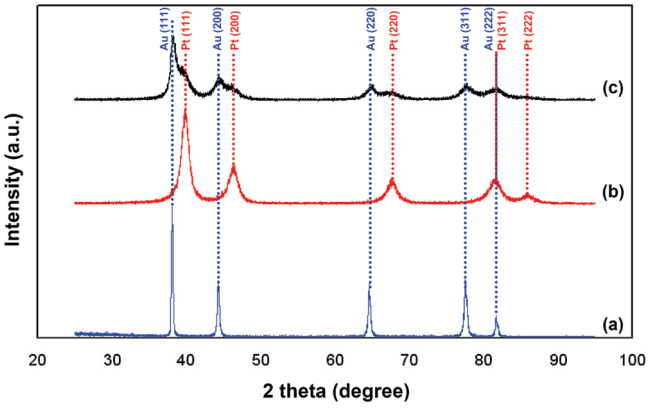

Figure 3. Wide-angle XRD patterns of (a) Au, (b) Pt, and (c) Au@Pt nanocolloids deposited in the presence of the F127 surfactant. The Au@Pt nanocolloids are prepared from a typical solution with a Pt/Au molar ratio of 1.0.

reduction potential, the reduction of Au ions preferentially occurs in a short time to produce Au cores. This is followed by overgrowth of the Pt dendritic nanowires on the Au seeds. During the Pt deposition, the Pluronic F127 plays an important role as a structural-directing agent, which has been previously reported by us.[21,23] It was shown that Pluronic surfactants such as P123 and F127 were critical for the formation of the dendritic Pt.[21,23] The poly(ethylene oxide) (PEO) group in poly(ethylene oxide)−poly(propylene oxide)−poly(ethylene oxide) (PEO−PPO−PEO) surfactants (Pluronic surfactants) is known to form a crown-ethers-like conformation, similar to a cavity structure in an aqueous solution. Because of the interaction between the hydrophobic PPO groups and the Pt surface, the Pluronic chains adsorbed on the Pt surface during the Pt deposition could form cavities and then facilitate the formation of the Pt dendrites. On the other hand, during the formation of the Au cores, the F127 cannot act as a structural-directing agent. Actually, the Au cores in the Au@Pt possess no nanostructures (see Figures 1a and 1b).

During the synthesis of the Au@Pt core−shell nanocolloids, we could easily monitor the progress of the synthesis through the evolution of the solution color. The color of the initial solution containing Au and Pt ions and F127 was yellow. As shown in Figure 4, after adding ascorbic acid (AA) solution and applying ultrasonic irradiation, the color gradually changed to burgundy, indicating that only the Au species were preferentially reduced to Au nanoparticles (Figure 4a). During the following 24 h, the solution gradually turned dark black, which is caused by growth of the Pt shells on the Au cores.

To further elucidate the synthesis progress, different stages of the formation of Au@Pt nanocolloids were observed by TEM. As shown in Figure 5, spherical Au nanoparticles were formed after 1 h reaction (Figure 5a). Enough nucleation sites for reduction of Pt ions are provided by the surface of the Au seeds. Gradual reduction of the Pt species led to the continuous nucleation and growth of Pt nanowires on the Au seed. After the formation of primary nanowires, secondary Pt nanowires grew on Au seeds and the primary Pt nanowires (Figure 5b), resulting in the formation of the dendritic Pt shell. The 6-h reaction was not sufficient to completely coat the Pt dendritic shell over the entire Au surface. In some parts, the exposed Au surface without the Pt shell was observed, as indicated by the arrow in Figure 5b. The growth of Pt shell continued until the complete consumption of Pt ions in solution (Figure 5c). At that time, the color of the solution changed to black (Figure 4). After a period of 24 h

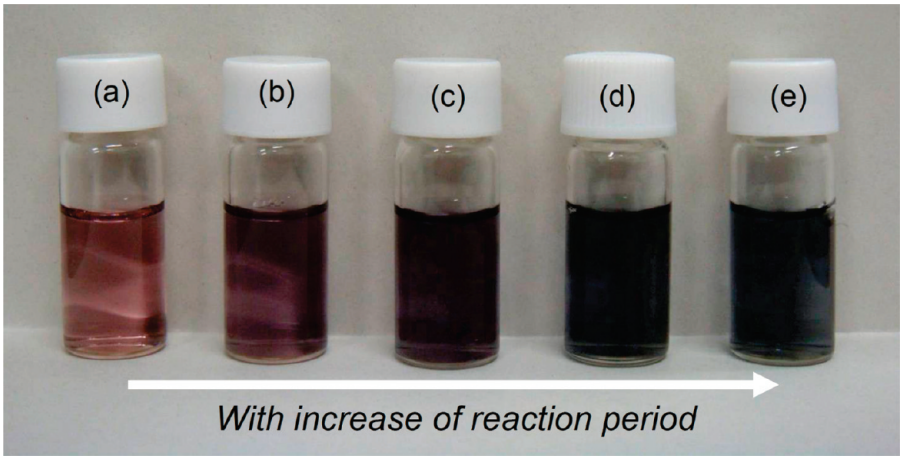

Figure 4. Photographs of colloidal suspensions taken at different reaction times: (a) 1 h, (b) 3 h, (c) 6 h, (d) 24 h, and (e) 48 h. After reaction for 24 h, the colors of the colloidal suspensions are not changed. The Pt/Au molar ratio used in the starting solution is 1.0.

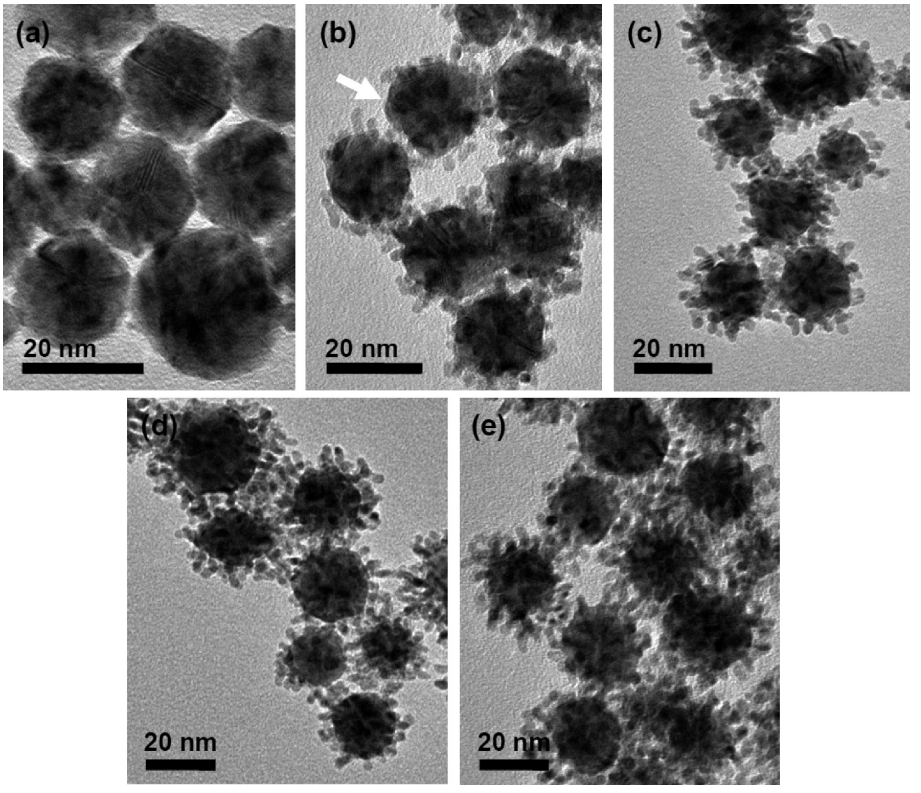

Figure 5. TEM images of samples taken at different reaction times: (a) 1 h, (b) 6 h, (c) 24 h, (d) 48 h, and (e) 72 h. After the reaction has proceeeded for 24 h, the morphology of the Au@Pt nanocolloids is not varied at all. The Pt/Au molar ratio used in the starting solution is 1.0. The position of the exposed Au surface without the Pt shell is indicated by the arrow.

following the start of the reaction, the growth of the Pt dendritic shell was terminated (see Figures 5d and 5e). The product morphology was not changed anymore (see Figures 5d and 5e).

The synthesis progress could be visibly monitored by UV−vis absorption spectroscopy at different reaction times (Figure 6). The solution after 1 h of reaction showed an extinction peak centered at 520 nm, originating from the Au surface plasmon (see Figures 6a and 6b).[40] As the Au seeds were covered with the dendritic Pt shell, the absorption peak gradually shifted to longer wavelengths (see Figures 6c−e). This red shift was accompanied by the suppression of the absorption peak, which was due to the formation of the dendritic Pt shell. These results confirmed a continuous overgrowth of the dendritic Pt shell on the surface of Au seed, which is consistent with TEM analysis (Figure 5). After the reaction for 24 h, the shape of the peaks was not changed at all, indicating that the reduction reaction of the metal species was terminated within 24 h.

The reaction time in the present study (24 h) was much longer rather than that of our previous study (<10 min).[39] In our previous study, Au@Pt core−shell nanocolloids with a very broad particle size distribution were

(40) Sakai, T.; Alexandridis, P. *J. Phys. Chem. B* **2005**, *109*, 7766.

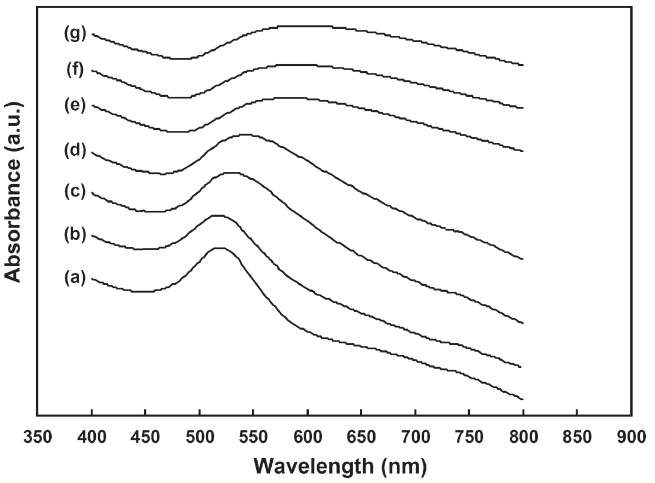

Figure 6. UV−vis absorption spectra of Au@Pt nanocolloids taken at different reaction times: (a) 30 min, (b) 1 h, (c) 3 h, (d) 6 h, (e) 24 h, (f) 48 h, and (g) 72 h. After 24 h of reaction, the shape of the peaks is not changed. The Pt/Au molar ratio used in the starting solution is 1.0.

prepared by using K_2PtCl_4 (as a Pt source) and $HAuCl_4$ (as a Au source).[39] According to the standard reduction potential of two Pt complexes (eqs 2 and 3), $[PtCl_6]^{2-}$ ions have a lower tendency toward reduction than $[PtCl_4]^{2-}$ ions. Therefore, replacing K_2PtCl_4 with H_2PtCl_6 greatly delays the reduction reaction of Pt complexes. In the present system, there is a large difference of the deposition potential of the Au and Pt salts. Therefore, the reduction of Au and Pt species can be completely separated in the reaction solutions, which is desirable for ideal one-step synthesis of a Au@Pt core−shell structure.

To examine the effect of ultrasonic treatment and different Pt/Au molar ratios in the solution, two series of experiments were performed. In one experiment, the precursor solutions with various molar ratios of Pt/Au (in the range of 0.00−4.00) were sonicated for 15 min in the presence of F127 and AA (see Figure 7). In another experiment, the ultrasonic treatment was replaced by mixing of the precursor solution with a magnetic stirrer (see Figure 8). Inductively copuled plasma (ICP) analysis showed that, in all of the samples, the composition of the Au@Pt nanocolloids was stoichiometrically consistent with the Pt/Au molar ratios in the starting solution, indicating that the amount of AA as a reducing agent is sufficient to completely reduce all of the Pt and Au species.

Figures 7 and 8 show TEM images of the Au@Pt nanocolloids synthesized by sonochemical reaction and using a stirring mixture, respectively. The Au@Pt nanocolloids prepared via sonochemical reaction had a smaller particle size with a narrow distribution, compared to those prepared by stirring mixture. The particle size distributions of the Au@Pt nanocolloids were investigated by counting more than 200 samples. As shown in Figure 9, the average size of the nanocolloids synthesized using the stirring mixture was 56 nm, with sizes ranging from 45 nm to 75 nm. In contrast, the size distribution of the nanocolloids prepared by sonochemical reaction was 20−35 nm, with an average size of 27 nm. By application of the ultrasonic irradiation, the average sizes were dramatically reduced and the particle size distribution became quite narrow.

As mentioned previously (Figures 5 and 6), primary Au seeds play the role of nucleation centers for growth of the Pt shell. The size and distribution of the final Au@Pt nanocolloids are dependent on those of Au seeds. Hence, the formation of Au cores with uniform size is necessary to create Au@Pt nanospheres with a narrow size distribution. The mechanism of the reduction of metal salts,[41−43] especially $HAuCl_4$,[44] could be generally explained by a model including a slow progressive nucleation and fast autocatalytic growth. The particle size and the width of the size distribution of the Au particles are inversely related to the number of the Au nuclei, which corresponds to the rate of nucleation.[45,46] In other words, when the number of the Au nuclei is smaller, the particle size has a tendency to increase and the size distribution broadens. This model can be adopted to explain the formation of Au seeds. In the mixture process that uses a magnetic stirrer, in the early stages of the reaction, Au seeds were slowly formed and served as nucleation centers. As the reduction reaction progressed, the formation of new seeds, combined with the autocatalytic growth of primary seeds, led to broadening of the particle size distribution. Finally, Au particle concentration reached a critical nucleus concentration and further seed formation was suppressed. Hence, the growth of Au predominates over the nucleation. In contrast, in the case of sonochemical reaction, the rate of Au reduction is significantly accelerated by the ultrasound radiation. Hence, instead of progressive nucleation during the reaction time, instantaneous nucleation occurs within a very short time. This means that the ratio of Au seeds to metal ions is dramatically increased, and a critical nucleus concentration is reached rapidly and further seeding is suppressed. Thus, small-sized Au nanoparticles with a narrow size distribution could be obtained. Recently, the use of high-intensity ultrasonics for the preparation of metal nanoparticles has been established by theoretical and experimental studies.[47−50] The ultrasonic-induced reduction is a result of acoustic cavitation, which involves the formation, growth, and implosive collapse of vacuum bubbles in solution. Within a collapsing bubble, the generation of transient high temperatures and pressures leads to a hemolytic dissociation of water and

(41) Chen, J. Y.; Herricks, T.; Geissler, M.; Xia, Y. N. *J. Am. Chem. Soc.* **2004**, *126*, 10854.
(42) Watzky, M. A.; Finke, R. G. *J. Am. Chem. Soc.* **1997**, *119*, 1038.
(43) Teng, X. W.; Liang, X. Y.; Maksimuk, S.; Yang, H. *Small* **2006**, *2*, 249.
(44) Jana, N. R.; Gearheart, L.; Murphy, C. J. *Chem. Mater.* **2001**, *13*, 2313.
(45) Okitsu, K.; Yue, A.; Tanabe, S.; Matsumoto, H.; Yobiko, Y.; Yoo, Y. *Bull. Chem. Soc. Jpn.* **2002**, *75*, 2289.
(46) Okitsu, K.; Ashokkumar, M.; Grieser, F. *J. Phys. Chem. B* **2005**, *109*, 20673.
(47) Mizukoshi, Y.; Oshima, R.; Maeda, Y.; Nagata, Y. *Langmuir* **1999**, *15*, 2733.
(48) Okitsu, K.; Ashokkumar, M.; Grieser, F. *J. Phys. Chem. B* **2005**, *109*, 20673.
(49) Margulis, M. A. *High Energy Chem.* **2004**, *38*, 135.
(50) Okitsu, K.; Yue, A.; Tanabe, S.; Matsumoto, H.; Yobiko, Y.; Yoo, Y. *Bull. Chem. Soc. Jpn.* **2002**, *75*, 2289.

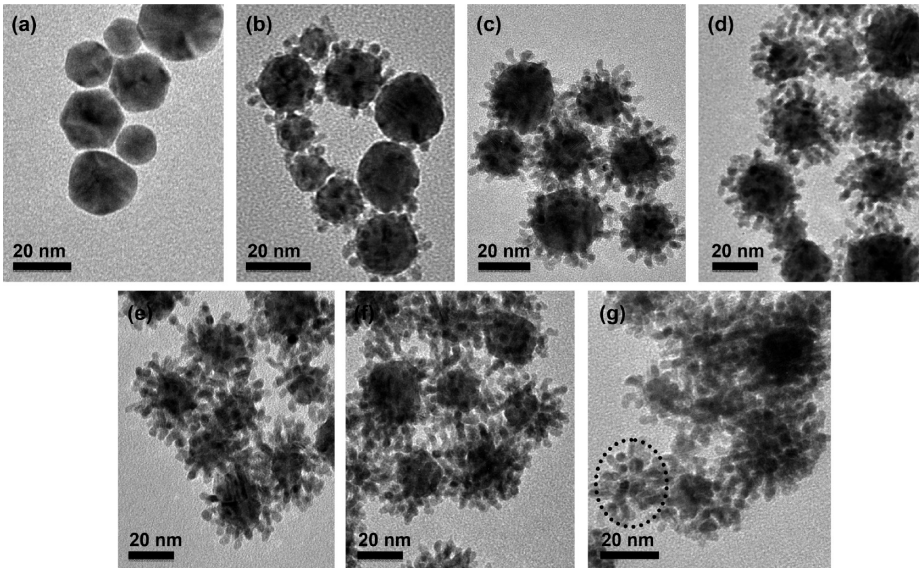

Figure 7. TEM images of (a) Au nanocolloids and (b−g) Au@Pt nanocolloids prepared by sonochemical reaction, using solutions with different Pt/Au molar ratios. The Pt/Au molar ratios are (a) 0.00, (b) 0.33, (c) 0.67, (d) 1.00, (e) 2.00, (f) 3.00, and (g) 4.00. The Pt nanodendrite without Au cores (as byproduct) is indicated by the dotted circle in panel (g).

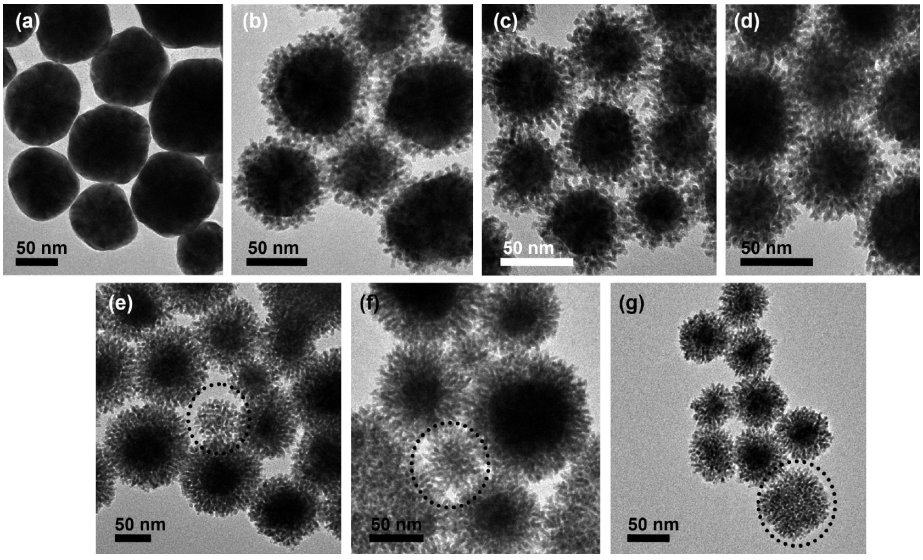

Figure 8. TEM images of (a) Au nanocolloids and (b−g) Au@Pt nanocolloids prepared via a stirring process, using solutions with different Pt/Au molar ratios. The Pt/Au molar ratios are (a) 0.00, (b) 0.33, (c) 0.67, (d) 1.00, (e) 2.00, (f) 3.00, and (g) 4.00. The Pt nanodendrite without Au cores (as byproduct) is indicated by a dotted circle in panels (e), (f), and (g).

other species to form reducing radicals.[51] Ultrasonic irradiation also provides not only high shear and stirring power but also homogeneous distribution of the mixing energy within the reaction volume without scale-up limitations. Consequently, instantaneous nucleation and homogeneous growth is induced by rapid reduction of the metal ions.[52,53] In the present sonochemical method, Au seeds with uniform size serve as nucleation centers for Pt sources, with the result that Au@Pt nanocolloids with uniform sizes were finally obtained.

Interestingly, the thicknesses of the Pt shell were easily tuned by varying the molar ratio of Pt/Au in the initial solutions (see Figure 10). The shell thicknesses of the prepared Au@Pt nanocolloids were measured from TEM images. In the experimental, the amounts of added Au solution were fixed to be 3.0 mL, whereas only the amounts of added Pt solutions were varied from 0 mL to 12 mL. (See Table 1 in the Experimental Section.) When the amount of Pt source was very small (1.0 mL) (i.e., the Pt/Au molar ratio is 0.33), several nanowires/nanoparticles with an average diameter of ~2 nm grew up to a few nanometers and were sparsely distributed on the Au cores. The Pt dendrites did not continuously cover the Au cores (see Figure 7b). With the increase of the Pt/Au molar ratios, the average thicknesses of the Pt shell were proportionally increased (see Figure 10).

(51) He, Y. H.; Vinodgopal, K.; Ashokkumar, M.; Greiser, F. *Res. Chem. Intermed.* **2006**, *32*, 709.
(52) Zhang, G. Q.; Wu, H. P.; Ge, M. Y.; Jiang, Q. K.; Chen, L. Y.; Yao, J. M. *Mater. Lett.* **2007**, *61*, 2204.
(53) Wu, C. W.; Mosher, B. P.; Zeng, T. F. *Chem. Mater.* **2006**, *18*, 2925.

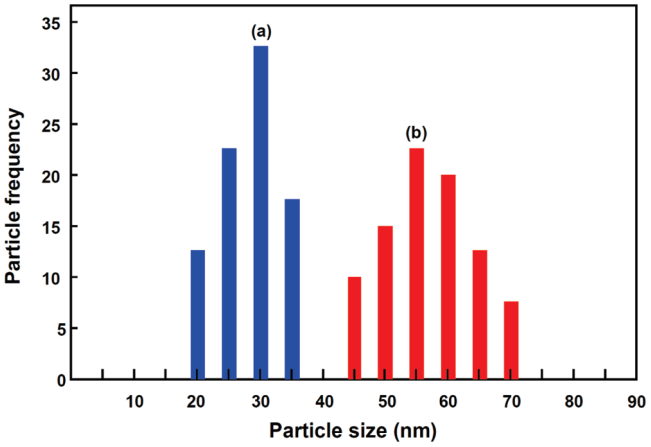

Figure 9. Particle size distributions of Au@Pt nanocolloids prepared by (a) sonochemical reaction and (b) stirring the mixture. The Pt/Au molar ratio used in the starting solution is 1.0.

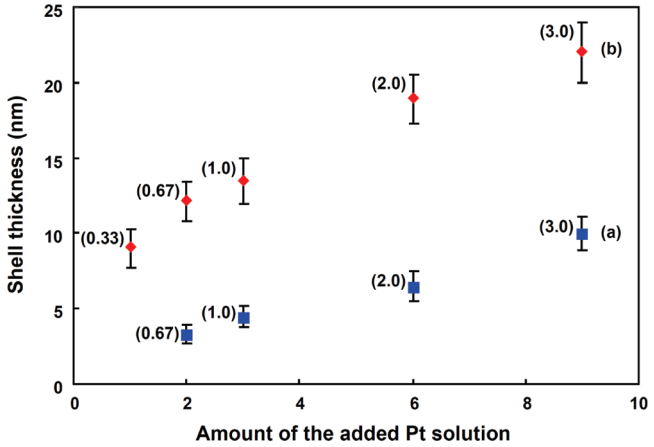

Figure 10. Relationship between the average Pt shell thicknesses and the added amount of Pt solutions. Au@Pt nanocolloids prepared by (a) sonochemical reaction and (b) stirring the mixture are compared. The Pt/Au molar ratios in the starting solutions are noted in parentheses.

In the case of stirring the mixture, when the Pt/Au molar ratio in the initial solution was further increased to 2.0, dendritic Pt particles without Au cores were confirmed as a byproduct in the TEM images (see Figure 8e). For Pt/Au molar ratios of more than 2.0, the amount of the byproduct was increased gradually as Pt/Au molar ratios were increased. However, in the case of the sonochemical reaction, no byproducts were observed until the Pt/Au molar ratio reached 4.00. This is because the size of the Au cores was decreased by the application of the ultrasonic irradiation (see Figures 7a and 8a), providing a larger Au exposed surface to volume.

The successful coating of the dendritic Pt shell on the Au core was characterized by UV−vis spectroscopy. Figure 11 shows the spectra of the Au@Pt nanocolloids from various solutions with different Pt/Au molar ratios. The Au nanocolloids without a Pt shell clearly showed an absorption peak centered at 520 nm, which was due to the surface plasmon resonance of Au nanocolloids (see Figure 11a). For Au@Pt nanocolloids with a Pt/Au molar ratio of 1.0, suppression and red shift of the absorption peak could be easily observed, because of overgrowth of the dendritic Pt shell. For higher Pt/Au molar ratios, the absorption peaks gradually diminish, because of the increasing Pt shell thickness.[38]

To demonstrate their potential uses as metal catalysts, the surface area of the Au@Pt nanocolloids was measured using N_2 adsorption−desorption isotherms (see Figure 12). The specific surface of the typical Au@Pt nanocolloids was 34 m^2/g, a value that is very close value to that of the dendritic Pt nanocolloids (32.9 m^2/g). Based on the Pt-mass normalization, the specific surface area of the Au@Pt nanocolloids was roughly calculated to be 68 $m^2/(g\ Pt)$, which is approximately twice as large as that of the dendritic Pt nanocolloids.

As a preliminary demonstration of the electrocatalytic ability of Au@Pt nanocolloids, the electrocatalytic activity toward the methanol oxidation reaction was tested using the CV method in 0.5 M H_2SO_4 + 0.5 M methanol solution. (See Figure 13.) The current densities were normalized by the loading amount of the Pt. The Au nanoparticles without the Pt shells as a reference had no

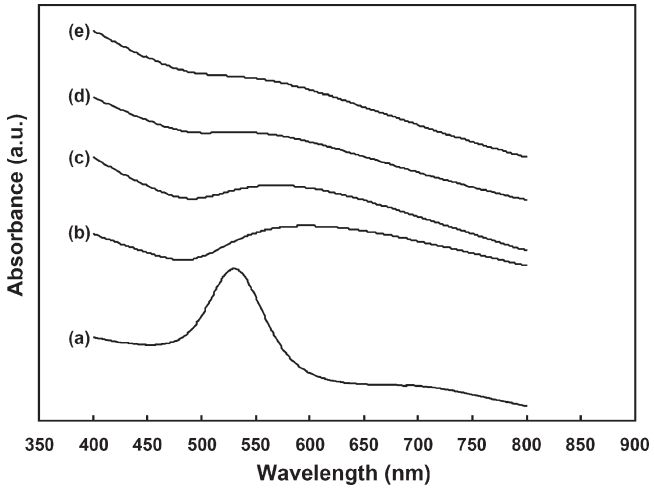

Figure 11. UV−vis absorption spectra of (a) Au nanocolloids and (b−e) Au@Pt nanocolloids prepared by sonochemical reaction, using the solutions with different Pt/Au molar ratios. The Pt/Au molar ratios are (a) 0.00, (b) 1.00, (c) 2.00, (d) 3.00, and (e) 4.00.

catalytic activity toward the oxidation of methanol. The Pt-mass-normalized activity of Au@Pt nanocolloids with Pt/Au molar ratios of 0.5 and 1.0 exhibited superior catalytic activity. These values were 85.8 and 116 mA/mg, respectively. However, with the further increase of Au/Pt molar ratios, the catalytic activity of Au@Pt nanocolloids is dramatically decreased. The Pt-mass normalized activity for the Au@Pt nanocolloids of Pt/Au molar ratios of 2.0 and 3.0 was 34.8 and 29.3 mA/mg, respectively. Consequently, the optimum Pt/Au molar ratio was determined to be 1.0. The obtained maximum electrocatalytic activity is ~4 times as large as that of the dendritic Pt nanoparticle without Au cores (28.5 mA/mg). The merit in the core−shell structures is the possibility of coating electrochemically active Pt thin layers. The efficiency of an electrocatalytic reaction is strongly dependent on the accessibility of the reactants to the catalysts.[38,54] In the Au@Pt nanocolloids with higher Pt/Au molar ratio or without a Au core, the methanol electrolyte cannot gain access to inner parts of the thick Pt shell. In other words, all of the Pt surface cannot work

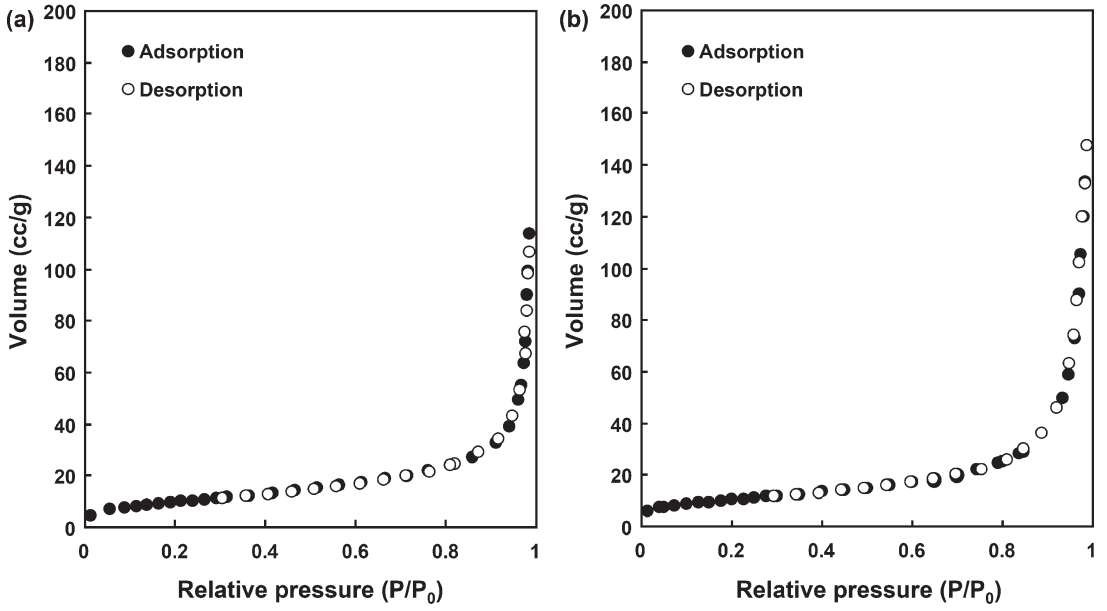

Figure 12. N_2 adsorption isotherms of (a) Au@Pt nanocolloids and (b) Pt dendritic nanocolloids prepared by sonochemical reaction. The Au@Pt nanocolloids are prepared from a typical solution with a Pt/Au molar ratio of 1.0.

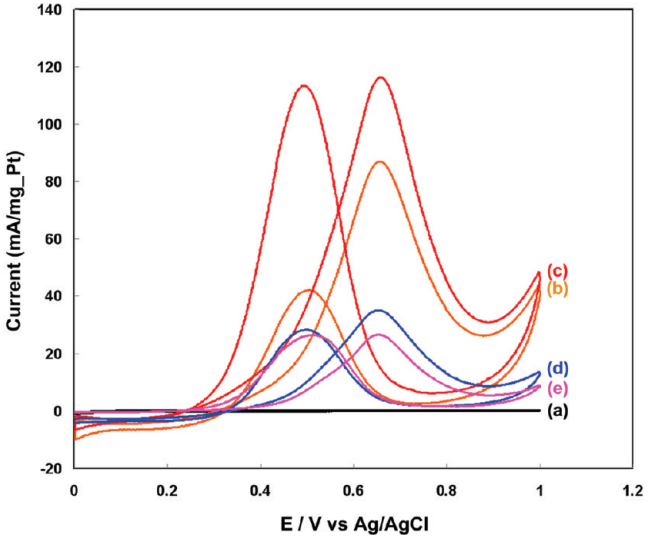

Figure 13. Pt-mass-normalized cyclic voltammograms (CVs) displaying the catalyzed oxidation of methanol, using (a) Au nanocolloids, (b–d) Au@Pt nanocolloids, and (e) Pt dendritic nanocolloids. The Au@Pt nanocolloids are prepared by sonochemical reaction using the solutions with different Pt/Au molar ratios of (b) 0.33 (c) 1.0, and (d) 2.0.

well as an electroactive surface. The enhancement of the catalytic activity is expected through the optimization of both the shell thicknesses and dimensions of the dendritic Pt layers.

4. Conclusion

The Au@Pt core–shell nanocolloids were successfully synthesized by chemical reduction of H_2PtCl_6 and $HAuCl_4$ salts under an aqueous low-concentration surfactant solution. Via the application of ultrasonic irradiation, the size of the Au@Pt nanocolloids was decreased and their particle size distribution became narrow, compared with the Au@Pt nanocolloids synthesized by stirring the mixture. Furthermore, the Pt dendritic shell thicknesses could be controlled by changing the Pt/Au molar ratios in the starting solutions. Through the careful optimization of the Pt shell thicknesses, the Pt-mass-normalized activity as an electrocatalyst for methanol oxidation reaction was drastically enhanced, which is ~4 times as large as that of the dendritic Pt nanocolloids without the Au cores. This is an important finding to improve the utilization efficiency of Pt catalysts in the future. The proposed method is a high-yield and low-cost pathway for metal-based core–shell structures, which have a large capability for scaleup.

Currently, inorganic core–shell structures have attracted interest as extensive research for integration of functionalities of both cores and shells.[55–59] Nanoporous/nanostructured materials with high surface areas have gained much attention as a promising candidate as shell materials.[55–60] However, the shell compositions have been mainly limited to nanoporous/nanostructured silica and carbon. In this paper, we have focused on metal-based core–shell structures with multifunctional architectures. This work can open new doors to creating novel metal-based core–shell structured materials with functional plasmonic, magnetic, and catalytic properties in the future.

Acknowledgment. One of the authors (L.W.) greatly appreciates the JSPS for support in the form of a fellowship at NIMS.

(54) Bruno, M. M.; Franceschini, E. A.; Planes, G. A.; Corti, H. R. *J. Appl. Electrochem.* **2010**, *40*, 257.
(55) Kim, J.; Lee, J. E.; Lee, J.; Yu, J. H.; Kim, B. C.; An, K.; Hwang, Y.; Shin, C. H.; Park, J. G.; Kim, J.; Hyeon, T. *J. Am. Chem. Soc.* **2006**, *128*, 688.
(56) Lin, Y. S.; Wu, S. H.; Hung, Y.; Chou, Y. H.; Chang, C.; Lin, M. L.; Tsai, C. P.; Mou, C. Y. *Chem. Mater.* **2006**, *18*, 5170.
(57) Giri, S.; Trewyn, B. G.; Stellmaker, M. P.; Lin, V. S. Y. *Angew. Chem., Int. Ed.* **2005**, *44*, 5038.
(58) Deng, Y.; Qi, D.; Deng, C.; Zhang, X.; Zhao, D. *J. Am. Chem. Soc.* **2008**, *130*, 28.
(59) Joo, S. H.; Park, J. Y.; Tsung, C. K.; Yamada, Y.; Yang, P. D.; Somorjai, G. A. *Nat. Mater.* **2009**, *8*, 126.
(60) Arnal, P. M.; Schüth, F.; Kleitz, F. *Chem. Commun.* **2006**, 1203.